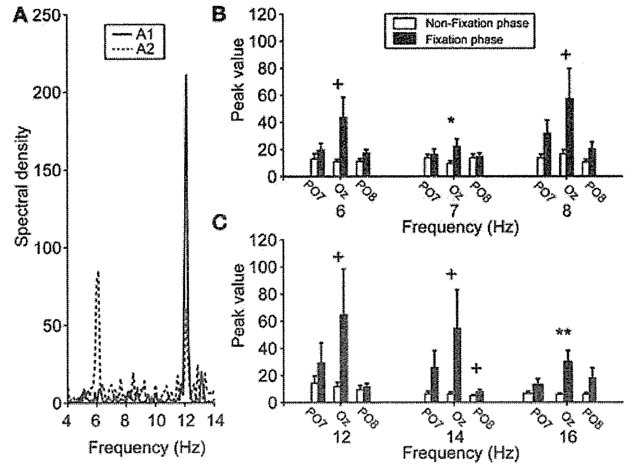

FIGURE 4 | SSVEP power during calibration. (A) Particular frequency spectra of EEG signals from Oz while fixating on the LED flicker at 6 Hz. Solid and dotted lines indicate the A1 and A2 results, respectively. The A1 spectrum revealed an increased frequency power at 12 Hz (i.e., a harmonic of 6 Hz), but A2 showed increases at both 6 and 12 Hz. **(B,C)** Mean spectral power of each electrode. Left, center, and right pair bars indicate the peak values of PO7, Oz, and PO8, respectively. Compared with the peak values during the non-fixation phase (white bars), those during the fixation phase (black bars), especially Oz, showed strengthening. Error bars indicate SE across participants. $^{+}p < 0.1$, $^{*}p < 0.05$, $^{**}p < 0.01$.

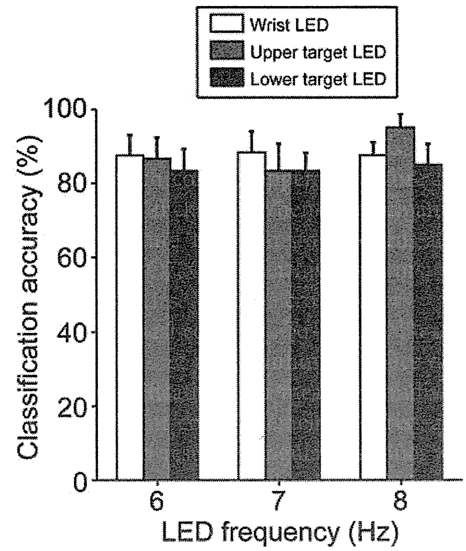

FIGURE 5 | Classification accuracy in BOTAS-assisted trials based on EEG signals from Oz. Accuracy was not dependent on the frequency or location of the LED flickers. Error bars indicate SE across participants.

was the principal SSVEP signal source (i.e., exhibiting a high SNR), relative to PO7 and PO8. In our efforts to construct a user-friendly BMI system, we sought to use as few electrodes as possible. Therefore, we used the EEG signal from Oz (only) to calibrate SVM and to perform online classification in BOTAS-assisted trials.

Classification accuracy

To evaluate the performance of the SSVEP-BMI system, we calculated the classification accuracy of EEG signals in BOTAS-assisted trials. Depending on the first classification into frequency classes (6, 7, or 8 Hz) during the fixation phase (phases B or D), we determined whether the classification in each trial was correct. If SVM first classified the EEG signal into any class other than the target frequency class-for example, despite a participant fixating on the LED flicker at 6 Hz, SVM classified the EEG signals into the 7 or 8 Hz class-the trial was defined as false.

The classification based on SVM was 80–90% accurate, on average, under all LED settings used (**Figure 5**). Only one participant (A10) yielded a poor classification accuracy (less than 70%, on average, across all LED settings) but most participants (8 of 12) exhibited good performance, with 90–100% classification accuracy (**Table 2**). To clarify the dependence of LED frequency and location on SVM performance, we performed Two-Way ANOVA (frequency of LED flickering × position of LED flickers). No significant main effect or interaction was apparent [frequency: $F_{(2, 22)} = 0.49$, $p = 0.62$; position: $F_{(2, 22)} = 0.95$, $p = 0.40$; interaction: $F_{(4, 44)} = 1.36$, $p = 0.26$].

Delay in SSVEP detection

Figure 6A shows the mean delay in SVM classification after participants fixated on any LED flicker in phases B or D. These delays indicate the time from LED fixation to driving of BOTAS. The results in **Figure 6A** are evaluation of only correct trials. The proportion of correct trials with respect to all trials was 88.5%. Using the LED setting associated with the shortest delay (frequency of LED flickering: 8 Hz, position of the LED flicker: lower target), SVM required about 2 s to classify the EEG correctly. At other LED settings, SSVEP also functioned correctly in less than 3 s. To clarify the dependence of LED frequency and location on SVM performance, repeated Two-Way ANOVA (frequency of LED flickering × position of the LED flickers) was used to analyze the delays (**Figure 6A**). ANOVA indicated that only the position of the LED flickers was significant [frequency: $F_{(2, 22)} = 0.23$; $p = 0.79$; position: $F_{(2, 22)} = 4.35$, $p < 0.05$; interaction: $F_{(4, 44)} = 0.45$, $p = 0.77$]. Additional analysis revealed a significant difference between the wrist and lower target LEDs ($p < 0.05$, Bonferroni test).

When participants fixated on any LED flicker during phases B or D, the detection rate increased with time (**Figure 6B**). The solid line indicates the detection rate in correct trials and the dotted line in all trials, included false trials. At 2 s after fixating, the detection rate increased sharply and the SVM classification for the grasping or reaching movement was success, 90.1% of correct trials and 85.8% of all trials within 5 s. Individual delays are shown in **Table 2**.

PATIENTS WITH UPPER CERVICAL SCI

Patients in this study did not have spasticity in the left arm; however, their arm joints showed narrower ROMs compared with the able-bodied participants. When patients participated in this task, we defined the task space based on the limited ROM.

Table 2 | Individual performances across all LED settings in able-bodied participants.

	A1	A2	A3	A4	A5	A6	A7	A8	A9	A10	A11	A12
CA (%)	98.3	98.3	80.0	96.7	90.0	91.7	93.3	98.3	75.0	65.0	96.7	78.3
Delay (s)	3.1	2.8	4.3	2.5	2.5	2.3	2.7	2.6	2.9	4.0	2.5	2.8

CA, Classification accuracy.

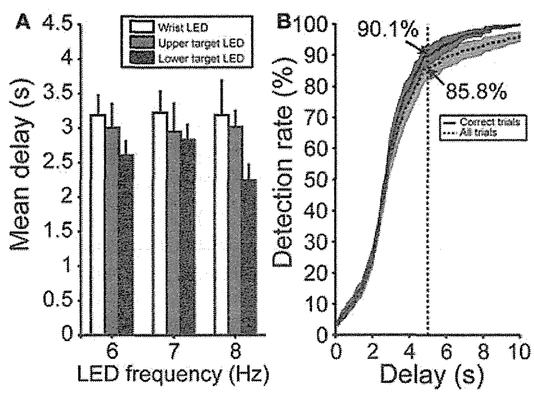

FIGURE 6 | Delay in initiation of BOTAS movement. (A) Mean delay from initiation of fixating on the LED flicker to driving BOTAS. These results were calculated based on correct trials. The delay was of slightly longer duration when the LED was attached to the participant's wrist. Error bars indicate SE across participants. **(B)** SSVEP detection rate after fixation on the LED flicker (*i.e.*, phases B and D). The results indicated by solid and dotted lines represent data calculated from correct trials and all trials, respectively. The BOTAS system began to detect SSVEP 2 s after initiation of fixating on the LED flicker. Participants successfully initiated grasping or reaching motions within 5 s in more than 85% of all trials.

Table 3 | Performance of patients in BOTAS-assisted trials.

Participant (Age, Gender, Time since injury, Injury level)	Classification accuracy (%)	Mean delay (s)	Detection rate within 5 s (%)
P1 (42, M, 16y, C6)	80.0	3.8	77.5
P2 (40, M, 19y, C3)	83.3	3.9	73.5
P3 (51, M, 24y, C6)	80.0	3.7	82.3

Table 3 shows the SVM performances of three patients with upper cervical SCI. Because Oz impedance in P1 did not decrease over time, the calibration and BOTAS-assisted trials featured high impedance. Classification accuracy and mean delay were slightly lower performance vs. those of the able-bodied participants. Accuracies were not less than 80% and delays were shorter than 4 s. We confirmed that the patients with upper cervical SCI operated the BOTAS system successfully. They successfully grasped the ball and transferred it to the goal position in a high proportion of trials (P1: 18/20 trials, P2: 29/30 trials, P3: 28/30 trials). No patient reported discomfort during task performance.

DISCUSSION

We prepared life-size robot arms BOTAS that can assist the wearer's goal-directed movements of the upper limb, such as reaching or grasping. To control the motion of the BOTAS, we recorded EEG signals. SSVEP was elicited, especially from Oz, during fixation on a LED flicker. In BOTAS-assisted trials, both able-bodied participants and patients with upper cervical SCIs successfully controlled the grasping-a-ball and carrying-the-ball movements in a high proportion of trials.

ASYNCHRONOUS CONTROL OF GOAL-DIRECTED MOVEMENTS

We developed the SSVEP-based BMI assist suit for the whole arm and fingers to support goal-directed actions involving multiple body parts, so that the devices could be used for movements such as those involved in OT training. Goal-directed activity has greater success in helping patients with paresis organize their movements effectively, compared with an exercise with no goal (Ma and Trombly, 2002; Pillastrini et al., 2008). Previous studies made use of rehabilitation robots with relatively high DOFs for shoulder and elbow motions (Sanchez et al., 2006; Ball et al., 2009; Dolce et al., 2009; Staubli et al., 2009) or finger motions (Schabowsky et al., 2010). However, providing a useful series of actions, such as reaching and grasping, was not easy using these robots. In this study, both able-bodied participants and patients with upper cervical SCIs successfully performed the grasping-a-ball and carrying-the-ball movements, which require not only shoulder and elbow motions but also wrist and finger motions, thus representing a purposeful and goal-directed movement. The effectiveness of movements used in rehabilitation training must be studied further, but our BOTAS system is suggested to be potentially useful for rehabilitation of patients with upper limb disabilities. In terms of clinical evaluation, it would be wise to evaluate user satisfaction (e.g., by applying the Quebec instrument evaluating satisfaction with assistive technology; QUEST 2.0) (Zickler et al., 2011).

In rehabilitation training using BMI technologies, an artificial closed-loop between the brain and the impaired body part(s) facilitates brain plasticity (Lebedev and Nicolelis, 2006; Gomez-Rodriguez et al., 2011). Additionally, synchronization between user intent and the action of the external device is important in BMI-based rehabilitation training. Recent invasive BMI technologies have succeeded in the asynchronous control of robot arms for useful series of actions, such as reaching and grasping (Hochberg et al., 2012). Several studies have used non-invasive BMI technologies to control assistive robots according to user intent (Muller-Putz and Pfurtscheller, 2008; Horki et al., 2010, 2011; Pfurtscheller et al., 2010b; Ortner et al., 2011). In this study, we prepared a pre-recorded series of useful actions-a grasping-a-ball movement and a carrying-the-ball movement—and provided asynchronous control using SSVEP signals. A SSVEP signal was used to trigger the grasping-a-ball movement and another SSVEP signal was used to trigger the carrying-the-ball movement. Although we did not attempt to directly decode user intention, participants fixated on LED flickers when they wished to start movement. Also, the hand and arm were visible when movements were made; this may have contributed to closed-loop sensory feedback. Asynchronous BMI systems using SSVEP may be useful for closed-loop rehabilitation approaches that make use of repetitive movement tasks (Horki et al., 2010; Diez et al., 2011; Ortner et al., 2011). Recent studies have further suggested that synchronization enabled by BMI between "motor intention of a wearer" and "motion of external device" render rehabilitation training effective (Ramos-Murguialday et al., 2013). In the BOTAS system, a wearer fixates on a LED flicker when she/he wants to drive motion, and BOTAS then comes into play. Thus, motor intention and BOTAS motion are synchronized. Previous studies suggest that our system will be effective in rehabilitation training, although further work is needed.

SSVEP FEATURES IN THE BOTAS SYSTEM

To construct a user-friendly BMI system, it is important that EEG signals are recorded using only a few electrodes (Luo and Sullivan, 2010). Many BMI systems in previous studies used multiple electrodes to detect SSVEP (Muller-Putz and Pfurtscheller, 2008; Horki et al., 2011; Ortner et al., 2011). Although use of multiple electrodes may facilitate detection of EEG signals and increase classification accuracy (Bin et al., 2009; Grave De Peralta Menendez et al., 2009; Bakardjian et al., 2010), multiple electrode placement requires considerable time, may burden users, and may be difficult to apply in rehabilitation training. Thus, practical BMI systems using small numbers of electrodes are potentially useful and may reduce user discomfort (Zickler et al., 2011). When recording EEG signals with a few electrodes, brain areas in which SSVEP is strongly induced should be focused on exclusively. SSVEP was not strong in lateral areas (for example, PO7 and PO8). Placement of electrodes in the central area, such as Oz, ought to be effective for SSVEP-BMIs (Pastor et al., 2003; Bin et al., 2008, 2009). Indeed, we found that the classification accuracy was over 80% using the EEG signal from Oz alone, but it would be valuable to further improve classification accuracy and decrease delay by optimizing the signal processing software and visual stimuli (i.e., hardware).

The colors and frequencies of visual stimuli are also important parameters for effective elicitation of SSVEP. Takano et al. (2009) reported that green/blue flicker stimuli improved EEG signal classification accuracy and the usability of the P300-based BMI system, compared with white/gray stimuli. This color tuning should also be effective in SSVEP-based BMIs. Further, SSVEP is strongly elicited at frequencies below ~20 Hz (Pastor et al., 2003; Bakardjian et al., 2010), and low-frequency LED flickers worked well in this study. Further work on optimization of visual stimuli is required.

The delay in SSVEP detection was affected by the LED location (wrist vs. target position). The delay was longer when the participants fixated on the LED flicker attached to their wrist, than in the other locations. Participants were asked to fixate on a LED flicker placed 80 cm away to yield EEG signal data permitting SVM calibration. Because the distance from the eyes of participants to the wrist-attached LED was ~40 cm, variation in the experimental setting (i.e., the location of LED flickers) will likely change perceived stimulus intensity or viewing angle, thus affecting the SSVEP response. On the other hand, the classification accuracies of the EEG signals from Oz did not depend on LED frequency or position. Thus, our BOTAS system exhibited robustness in terms of EEG classification and allowed the LED parameters (frequency, location) to be set according to the task or environment.

In this study, the participants were able to control BOTAS successfully using SSVEP. The system could be operated with little training and BOTAS could be driven asynchronously whenever the wearer wished to. EEG signals recorded from the visual cortex (Oz) were used in classification. The data indicate that our BOTAS system is potentially useful in rehabilitation of patients with upper limb disabilities. Future work, including unit downsizing, will allow us to develop an intelligent orthosis useful in terms of daily life support.

ACKNOWLEDGMENTS

This study was supported in part by a Grant-in-Aid from the Ministry of Health, Labor and Welfare to Kenji Kansaku (Japan). We thank Drs. H. Kurumadani and K. Yamaguchi for their help and Drs. Y. Nakajima and S. Kato for their encouragement. We also thank Oki Electric Industry Co., Ltd. and Oki Information Systems Co., Ltd. for BOTAS development.

REFERENCES

Allison, B. Z., Brunner, C., Kaiser, V., Muller-Putz, G. R., Neuper, C., and Pfurtscheller, G. (2010). Toward a hybrid brain-computer interface based on imagined movement and visual attention. *J. Neural Eng.* 7:26007. doi: 10.1088/1741-2560/7/2/026007

Amirabdollahian, F., Loureiro, R., Gradwell, E., Collin, C., Harwin, W., and Johnson, G. (2007). Multivariate analysis of the Fugl-Meyer outcome measures assessing the effectiveness of GENTLE/S robot-mediated stroke therapy. *J. Neuroeng. Rehabil.* 4, 4. doi: 10.1186/1743-0003-4-4

Bakardjian, H., Tanaka, T., and Cichocki, A. (2010). Optimization of SSVEP brain responses with application to eight-command Brain-Computer Interface. *Neurosci. Lett.* 469, 34–38. doi: 10.1016/j.neulet.2009.11.039

Ball, S. J., Brown, I. E., and Scott, S. H. (2009). Performance evaluation of a planar 3DOF robotic exoskeleton for motor assessment. *J. Med. Device* 3, 21002. doi: 10.1115/1.3131727

Bastos, T. F., Muller, S. M., Benevides, A. B., and Sarcinelli-Filho, M. (2011). Robotic wheelchair commanded by SSVEP, motor imagery and word generation. *Conf. Proc. IEEE Eng. Med. Biol. Soc.* 2011, 4753–4756. doi: 10.1109/IEMBS.2011.6091177

Bin, G., Gao, X., Yan, Z., Hong, B., and Gao, S. (2009). An online multi-channel SSVEP-based brain-computer interface using a canonical correlation analysis method. *J. Neural Eng.* 6:046002. doi: 10.1088/1741-2560/6/4/046002

Bin, G., Lin, Z., Gao, X., Hong, B., and Gao, S. (2008). The SSVEP topographic scalp maps by canonical correlation analysis. *Conf. Proc. IEEE Eng. Med. Biol. Soc.* 2008, 3759–3762. doi: 10.1109/IEMBS. 2008.4650026

Birbaumer, N., and Cohen, L. G. (2007). Brain-computer interfaces: communication and restoration of movement in paralysis. *J. Physiol.* 579, 621–636. doi: 10.1113/jphysiol.2006.125633

Cheng, M., Gao, X., Gao, S., and Xu, D. (2002). Design and implementation of a brain-computer interface with high transfer rates. *IEEE Trans. Biomed. Eng.* 49, 1181–1186. doi: 10.1109/TBME. 2002.803536

Collinger, J. L., Wodlinger, B., Downey, J. E., Wang, W., Tyler-Kabara, E. C., Weber, D. J., et al. (2013). High-performance neuroprosthetic control by an individual with tetraplegia. *Lancet* 381, 557–564. doi: 10.1016/S0140-6736(12) 61816-9

Diez, P. F., Mut, V. A., Avila Perona, E. M., and Laciar Leber, E. (2011). Asynchronous BCI control using high-frequency SSVEP. *J. Neuroeng. Rehabil.* 8, 39. doi: 10.1186/1743-0003-8-39

Dipietro, L., Ferraro, M., Palazzolo, J. J., Krebs, H. I., Volpe, B. T., and Hogan, N. (2005). Customized interactive robotic treatment for stroke: EMG-triggered therapy. *IEEE Trans. Neural Syst. Rehabil. Eng.* 13, 325–334. doi: 10.1109/ TNSRE.2005.850423

Dolce, G., Lucca, L. F., and Pignolo, L. (2009). Robot-assisted rehabilitation of the paretic upper limb: rationale of the ARAMIS project. *J. Rehabil. Med.* 41, 1007–1101. doi: 10.2340/16501977-0406

Farwell, L. A., and Donchin, E. (1988). Talking off the top of your head: toward a mental prosthesis utilizing event-related brain potentials. *Electroencephalogr. Clin. Neurophysiol.* 70, 510–523. doi: 10.1016/0013-4694(88)90149-6

Finley, M. A., Fasoli, S. E., Dipietro, L., Ohlhoff, J., Macclellan, L., Meister, C., et al. (2005). Short-duration robotic therapy in stroke patients with severe upper-limb motor impairment. *J. Rehabil. Res. Dev.* 42, 683–692. doi: 10.1682/JRRD.2004.12.0153

Flash, T., and Hogan, N. (1985). The coordination of arm movements: an experimentally confirmed mathematical model. *J. Neurosci.* 5, 1688–1703.

Gomez-Rodriguez, M., Peters, J., Hill, J., Scholkopf, B., Gharabaghi, A., and Grosse-Wentrup, M. (2011). Closing the sensorimotor loop: haptic feedback facilitates decoding of motor imagery. *J. Neural Eng.* 8:036005. doi: 10.1088/1741-2560/8/3/036005

Grave De Peralta Menendez, R., Dias, J. M. M., Prado, J.A.S., Aliakbarpour, H., and Gonzalez Andino, S. (2009). "Multiclass brain computer interface based on visual attention," in *European Symposium on Artificial Neural Networks—Advances in Computational Intelligence and Learning*, (Bruges), 22–24.

Hesse, S., Mehrholz, J., and Werner, C. (2008). Robot-assisted upper and lower limb rehabilitation after stroke: walking and arm/hand function. *Dtsch. Arztebl. Int.* 105, 330–336. doi: 10.3238/arztebl.2008. 0330

Hochberg, L. R., Bacher, D., Jarosiewicz, B., Masse, N. Y., Simeral, J. D., Vogel, J., et al. (2012). Reach and grasp by people with tetraplegia using a neurally controlled robotic arm. *Nature* 485, 372–375. doi: 10.1038/nature11076

Horki, P., Neuper, C., Pfurtscheller, G., and Muller-Putz, G. (2010). Asynchronous steady-state visual evoked potential based BCI control of a 2-DoF artificial upper limb. *Biomed. Tech. (Berl.)* 55, 367–374. doi: 10.1515/bmt.2010.044

Horki, P., Solis-Escalante, T., Neuper, C., and Muller-Putz, G. (2011). Combined motor imagery and SSVEP based BCI control of a 2 DoF artificial upper limb. *Med. Biol. Eng. Comput.* 49, 567–577. doi: 10.1007/s11517-011-0750-2

Ikegami, S., Takano, K., Saeki, N., and Kansaku, K. (2011). Operation of a P300-based brain-computer interface by individuals with cervical spinal cord injury. *Clin. Neurophysiol.* 122, 991–996. doi: 10.1016/j.clinph.2010.08.021

Kansaku, K. (2011). "Brain-machine interfaces for persons with disabilities," in *Systems Neuroscience and Rehabilitation*, eds K. Kansaku and L. G. Cohen (Berlin: Springer), 19–33. doi: 10.1007/978-4-431-540 08-3_2

Krebs, H. I., Dipietro, L., Volpe, B. T., and Hogan, N. (2003). Rehabilitation robotics: performance-based progressive robot-assisted therapy. *Auton. Robots* 15, 7–20. doi: 10.1023/A:102 4494031121

Krebs, H. I., Volpe, B. T., Williams, D., Celestino, J., Charles, S. K., Lynch, D., et al. (2007). Robot-aided neurorehabilitation: a robot for wrist rehabilitation. *IEEE Trans. Neural Syst. Rehabil. Eng.* 15, 327–335. doi: 10.1109/TNSRE.2007.903899

Lebedev, M. A., and Nicolelis, M. A. (2006). Brain-machine interfaces: past, present and future. *Trends Neurosci.* 29, 536–546. doi: 10.1016/j.tins.2006.07.004

Luo, A., and Sullivan, T. J. (2010). A user-friendly SSVEP-based brain-computer interface using a time-domain classifier. *J. Neural Eng.* 7:26010. doi: 10.1088/1741-2560/7/ 2/026010

Ma, H. I., and Trombly, C. A. (2002). A synthesis of the effects of occupational therapy for persons with stroke, Part II: remediation of impairments. *Am. J. Occup. Ther.* 56, 260–274. doi: 10.5014/ajot.56.3.260

Marchal-Crespo, L., and Reinkensmeyer, D. J. (2009). Review of control strategies for robotic movement training after neurologic injury. *J. Neuroeng. Rehabil.* 6, 20. doi: 10.1186/1743-0003-6-20

Masiero, S., Armani, M., and Rosati, G. (2011). Upper-limb robot-assisted therapy in rehabilitation of acute stroke patients: focused review and results of new randomized controlled trial. *J. Rehabil. Res. Dev.* 48, 355–366. doi: 10.1682/JRRD.2010.04.0063

Muller-Putz, G. R., and Pfurtscheller, G. (2008). Control of an electrical prosthesis with an SSVEP-based BCI. *IEEE Trans. Biomed. Eng.* 55, 361–364. doi: 10.1109/TBME.2007. 897815

Muller, S. M., Celeste, W. C., Bastos-Filho, T. F., and Sarcinelli-Filho, M. (2010). Brain-computer interface based on visual evoked potentials to command autonomous robotic wheelchair. *J. Med. Biol. Eng.* 30, 407–416. doi: 10.5405/ jmbe.765

Ortner, R., Allison, B. Z., Korisek, G., Gaggl, H., and Pfurtscheller, G. (2011). An SSVEP BCI to control a hand orthosis for persons with tetraplegia. *IEEE Trans. Neural Syst. Rehabil. Eng.* 19, 1–5. doi: 10.1109/TNSRE.2010.2076364

Panicker, R. C., Puthusserypady, S., and Sun, Y. (2011). An asynchronous P300 BCI with SSVEP-based control state detection. *IEEE Trans. Biomed. Eng.* 58, 1781–1788. doi: 10.1109/TBME.2011.2116018

Pastor, M. A., Artieda, J., Arbizu, J., Valencia, M., and Masdeu, J. C. (2003). Human cerebral activation during steady-state visual-evoked responses. *J. Neurosci.* 23, 11621–11627.

Pfurtscheller, G., Allison, B. Z., Brunner, C., Bauernfeind, G., Solis-Escalante, T., Scherer, R., et al. (2010a). The hybrid BCI. *Front. Neurosci.* 4:30. doi: 10.3389/fnpro.2010.00003

Pfurtscheller, G., Solis-Escalante, T., Ortner, R., Linortner, P., and Muller-Putz, G. R. (2010b). Self-paced operation of an SSVEP-Based orthosis with and without an imagery-based "brain switch:" a feasibility study towards a hybrid BCI. *IEEE Trans. Neural Syst. Rehabil. Eng.* 18, 409–414. doi: 10.1109/TNSRE.2010.2040837

Pichiorri, F., De Vico Fallani, F., Cincotti, F., Babiloni, F., Molinari, M., Kleih, S. C., et al. (2011). Sensorimotor rhythm-based brain-computer interface training: the impact on motor cortical responsiveness. *J. Neural Eng.* 8, 025020. doi: 10.1088/1741-2560/8/2/025020

Pignolo, L. (2009). Robotics in neuro-rehabilitation. *J. Rehabil. Med.* 41, 955–960. doi: 10.2340/16501977-0434

Pillastrini, P., Mugnai, R., Bonfiglioli, R., Curti, S., Mattioli, S., Maioli, M. G., et al. (2008). Evaluation of an occupational therapy program for patients with spinal cord injury. *Spinal Cord* 46, 78–81. doi: 10.1038/sj.sc.3102072

Ramos-Murguialday, A., Broetz, D., Rea, M., Laer, L., Yilmaz, O., Brasil, F. L., et al. (2013). Brain-machine interface in chronic stroke rehabilitation: a controlled study. *Ann. Neurol.* 74, 100–108. doi: 10.1002/ ana.23879

Regan, D. (1989). *Human Brain Electrophysiology: Evoked Potentials and Evoked Magnetic Fields in Science and Medicine.* New York, NY: Elsevier.

Sakurada, T., Takano, K., and Kansaku, K. (2011). "A BCI-based OT-assist suit for paralyzed upper extremities: a combination of sensorimotor rhythm, P300 and SSVEP," in *Program No. 142.09. 2011 Neuroscience Meeting Planner*, (Washington, DC: Society for Neuroscience) [online].

Sanchez, R. J., Liu, J., Rao, S., Shah, P., Smith, R., Rahman, T., et al. (2006). Automating arm movement training following severe stroke: functional exercises with quantitative feedback in a gravity-reduced environment. *IEEE Trans. Neural Syst. Rehabil. Eng.* 14, 378–389. doi: 10.1109/TNSRE. 2006.881553

Schabowsky, C. N., Godfrey, S. B., Holley, R. J., and Lum, P. S. (2010). Development and pilot testing of HEXORR: hand EXOskeleton rehabilitation robot. *J. Neuroeng. Rehabil.* 7, 36. doi: 10.1186/1743-0003-7-36

Song, R., Tong, K. Y., Hu, X., and Li, L. (2008). Assistive control system using continuous myoelectric signal in robot-aided arm training for patients after stroke. *IEEE Trans. Neural Syst. Rehabil. Eng.* 16, 371–379. doi: 10.1109/TNSRE.2008.926707

Staubli, P., Nef, T., Klamroth-Marganska, V., and Riener, R. (2009). Effects of intensive arm training with the rehabilitation robot ARMin II in chronic stroke patients: four single-cases. *J. Neuroeng. Rehabil.* 6, 46. doi: 10.1186/1743-0003-6-46

Takano, K., Hata, N., and Kansaku, K. (2011). Towards intelligent environments: an augmented reality-brain-machine interface operated with a see-through head-mount display. *Front. Neurosci.* 5:60. doi: 10.3389/fnins.2011.00060

Takano, K., Komatsu, T., Hata, N., Nakajima, Y., and Kansaku, K. (2009). Visual stimuli for the P300 brain-computer interface: a comparison of white/gray and green/blue flicker matrices. *Clin. Neurophysiol.* 120, 1562–1566. doi: 10.1016/j.clinph.2009.06.002

Trejo, L. J., Rosipal, R., and Matthews, B. (2006). Brain-computer interfaces for 1-D and 2-D cursor control: designs using volitional control of the EEG spectrum or steady-state visual evoked potentials. *IEEE Trans. Neural Syst. Rehabil. Eng.* 14, 225–229. doi: 10.1109/TNSRE.2006.875578

Uno, Y., Kawato, M., and Suzuki, R. (1989). Formation and control of optimal trajectory in human multijoint arm movement. Minimum torque-change model. *Biol. Cybern.* 61, 89–101. doi: 10.1007/BF00204593

Vapnik, V. (1996). *The Nature of Statistical Learning Theory*. Berlin: Springer.

Volosyak, I. (2011). SSVEP-based Bremen-BCI interface—boosting information transfer rates. *J. Neural Eng.* 8:036020. doi: 10.1088/1741-2560/8/3/036020

Wang, Y., Wang, R., Gao, X., Hong, B., and Gao, S. (2006). A practical VEP-based brain-computer interface. *IEEE Trans. Neural Syst. Rehabil. Eng.* 14, 234–239. doi: 10.1109/TNSRE.2006.875576

Wilson, J. J., and Palaniappan, R. (2011). Analogue mouse pointer control via an online steady state visual evoked potential (SSVEP) brain-computer interface. *J. Neural Eng.* 8:025026. doi: 10.1088/1741-2560/8/2/025026

Wolbrecht, E. T., Chan, V., Reinkensmeyer, D. J., and Bobrow, J. E. (2008). Optimizing compliant, model-based robotic assistance to promote neurorehabilitation. *IEEE Trans. Neural Syst. Rehabil. Eng.* 16, 286–297. doi: 10.1109/TNSRE.2008.918389

Wolpaw, J. R., Birbaumer, N., McFarland, D. J., Pfurtscheller, G., and Vaughan, T. M. (2002). Brain-computer interfaces for communication and control. *Clin. Neurophysiol.* 113, 767–791. doi: 10.1016/S1388-2457(02)00057-3

Zhu, D., Bieger, J., Garcia Molina, G., and Aarts, R. M. (2010). A survey of stimulation methods used in SSVEP-based BCIs. *Comput. Intell. Neurosci.* 2010:702357. doi: 10.1155/2010/702357

Zickler, C., Riccio, A., Leotta, F., Hillian-Tress, S., Halder, S., Holz, E., et al. (2011). A brain-computer interface as input channel for a standard assistive technology software. *Clin. EEG Neurosci.* 42, 236–244. doi: 10.1177/155005941104200409

Conflict of Interest Statement: The authors declare that the research was conducted in the absence of any commercial or financial relationships that could be construed as a potential conflict of interest.

Received: 01 May 2013; accepted: 03 September 2013; published online: 23 September 2013.

Citation: Sakurada T, Kawase T, Takano K, Komatsu T and Kansaku K (2013) A BMI-based occupational therapy assist suit: asynchronous control by SSVEP. Front. Neurosci. 7:172. doi: 10.3389/fnins.2013.00172

This article was submitted to Neuroprosthetics, a section of the journal Frontiers in Neuroscience.

Journal of Integrative Neuroscience, Vol. 12, No. 3 (2013) 331–341

DOI: 10.1142/S0219635213500192

Imperial College Press
www.icpress.co.uk

Implementation of a beam forming technique in real-time magnetoencephalography

Hiroki Ora[*,†], Kouji Takano[*], Toshihiro Kawase[*], Sunao Iwaki[‡,§], Lauri Parkkonen[¶] and Kenji Kansaku[*,§,||]

[*]*Systems Neuroscience Section, Department of Rehabilitation for Brain Functions Research Institute of National Rehabilitation Center for Persons with Disabilities Tokorozawa 359-8555, Japan*

[†]*Department of Computational Intelligence and Systems Science Tokyo Institute of Technology, Yokohama 226-8503, Japan*

[‡]*AIST Tsukuba Central 6, 1-1-1 Higashi, Tsukuba Ibaraki 305-8566, Japan*

[§]*Research Center for Frontier Medical Engineering, Chiba University Chiba 263-8522, Japan*

[¶]*Department of Biomedical Engineering and Computational Science (BECS) Aalto University, School of Science, 00076 Espoo, Finland*

[||]*kansaku-kenji@rehab.go.jp*

[Received 6 February 2013; Accepted 3 June 2013; Published 2 September 2013]

Real-time magnetoencephalography (rtMEG) is an emerging neurofeedback technology that could potentially benefit multiple areas of basic and clinical neuroscience. In the present study, we implemented voxel-based real-time coherence measurements in a rtMEG system in which we employed a beamformer to localize signal sources in the anatomical space prior to computing imaginary coherence. Our rtMEG experiment showed that a healthy subject could increase coherence between the parietal cortex and visual cortex when attending to a flickering visual stimulus. This finding suggests that our system is suitable for neurofeedback training and can be useful for practical brain–machine interface applications or neurofeedback rehabilitation.

Keywords: Real-time MEG; beam forming; imaginary coherence; neurofeedback.

1. Introduction

Real-time feedback of brain activity is potentially useful in multiple areas of basic and clinical research such as in rehabilitation and more recently, in brain–machine interfacing. Real-time neurofeedback of brain activity was first studied in the late 1960s to induce voluntary control of electroencephalogram (EEG) components at specific frequency bands (Kamiya, 1968) and also to control slow cortical potentials

[||]Corresponding author.

(Birbaumer *et al.*, 1990). EEG neurofeedback has been used to treat patient groups such as children with attention deficit hyperactivity disorder (ADHD) (Konrad & Eickhoff, 2010); however, limited spatial resolution is a drawback of this technique.

The development of blood oxygen level-dependent (BOLD) functional magnetic resonance imaging (fMRI), which has high spatial resolution (on the scale of a few mm), and new data acquisition and processing techniques enabled research into real-time fMRI-based neurofeedback (Caria *et al.*, 2012; Weiskopf *et al.*, 2003; Shibata *et al.*, 2011). fMRI neurofeedback studies use the data of real-time brain activity from specific regions of interest (ROI) for the feedback. However, because fMRI measures the hemodynamic response to neural activity based on changes in blood oxygenation, the temporal resolution of the signals is limited.

The temporal signal features of the magnetoencephalogram (MEG) are similar to those of the EEG and have been used in neurofeedback studies (Mellinger *et al.*, 2007; Buch *et al.*, 2008; Sudre *et al.*, 2011; Sacchet *et al.*, 2012). Most MEG-based neurofeedback protocols employ the MEG signals at the sensor level, i.e., without source models. However, since the MEG sensors are relatively distant from the sources and not all sensor types show the maximum sensitivity to sources right beneath them, and the signal at the sensor position does not directly correspond to neural activity in the specific brain area, thus, sensor-level analysis of MEG is limited in terms of the localization of neural activity. Feedback based on the activity in a specific, anatomically-defined ROI would be most desirable for neurofeedback studies.

The present real-time MEG (rtMEG) study employed a linearly-constrained minimum-variance (LCMV) beamformer, a form of spatial filtering (Van Veen & Kevin, 1988; Van Veen *et al.*, 1997), to improve the localization of neural activity beyond sensor-level analysis. The combination of the beamformer and anatomical MRIs allowed us to estimate neural currents in the individual gray matter. Thus, sensor-level signals were transformed into cortical source-level signals that are bound to anatomical brain structures.

Human cognition is considered to result from the interaction of multiple brain areas. Thus, understanding functional connectivity is necessary to understand cognitive processing (Siegel *et al.*, 2012). Here, we specifically focused on imaginary coherence to estimate functional connectivity between brain regions (Nolte *et al.*, 2004). The rationale of using imaginary coherence comes from the fact that linear synchronization measures may report false correlations due to spatial leakage of the source estimate. However, the "true" correlation among brain regions often contains a lag due to neural transmission. Thus, omitting the real part of coherency is expected to remove false correlations (Nolte *et al.*, 2004).

The present study is the first to report a novel rtMEG system in which real-time beamformer processing, used to improve localization of the signal source beyond what can be reached in sensor-level analysis, was combined with imaginary coherence estimation.

2. Materials and Methods

2.1. *System structure and signal processing chain*

The hardware structure of the system and the flow chart of real-time signal processing are shown in Figs. 1 and 2, respectively. The MEG scanner was a 306-channel Elekta Neuromag system (Elekta Oy, Helsinki, Finland). MEG signals were transferred from the system electronics to a workstation (Hewlett–Packard 64-bit, running Red Hat Linux) via an Ethernet-based TCP/IP connection (not shown in the figure). On the workstation, signal-space projection (SSP) was applied to reduce external interference and the signals were accumulated in the Field Trip real-time buffer (Sudre *et al.*, 2011; Oostenveld *et al.*, 2011) and then transferred using transmission control protocol (TCP) to a notebook computer (MacBook Pro, Apple Inc., Cupertino, CA, USA). The SSP operator was determined by applying principal component analysis (PCA) to data acquired in the absence of any subject and selecting four principal components for the magnetometer channels and 5 s for the planar gradiometer channels.

The MEG signal was reconstructed into an anatomical-location-based signal in the notebook computer by applying a spatial filter based on the LCMV beamformer (Van Veen & Kevin, 1988; Van Veen *et al.*, 1997) as described. The putative functional connectivity between two ROIs was estimated by calculating the imaginary

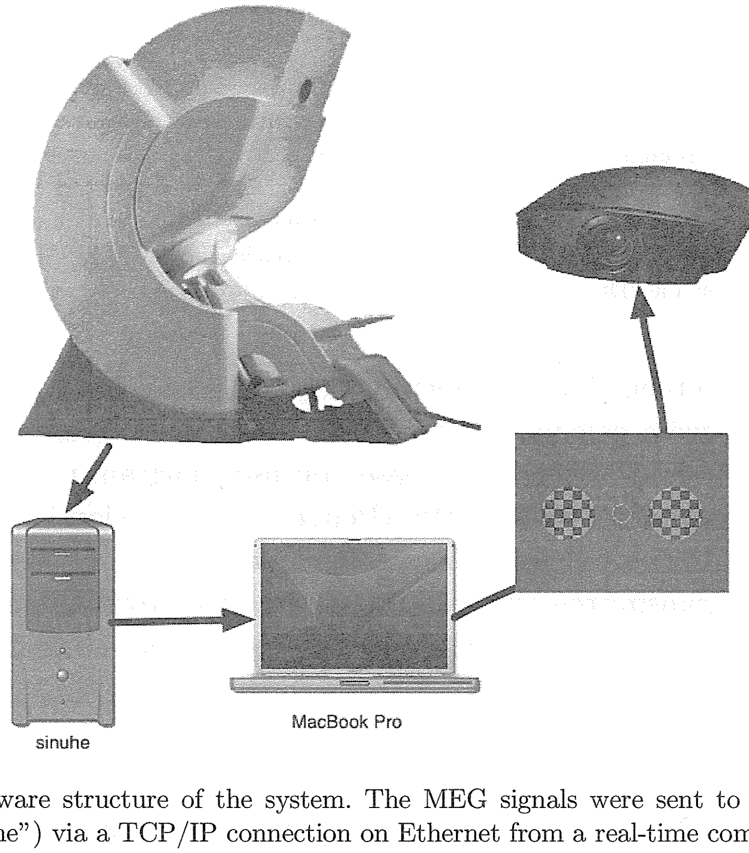

Fig. 1. The hardware structure of the system. The MEG signals were sent to the data acquisition workstation ("sinuhe") via a TCP/IP connection on Ethernet from a real-time computer (internal component of the MEG system; *not shown*) and accumulated into a buffer in a shared memory segment. The signals were then transferred in packets of 10,000 samples using TCP on Ethernet to a notebook computer (MacBook Pro) in which the functional connectivity was estimated and the visual feedback was generated based on those estimates. Visual feedback was then sent to the projector and displayed to the subject.

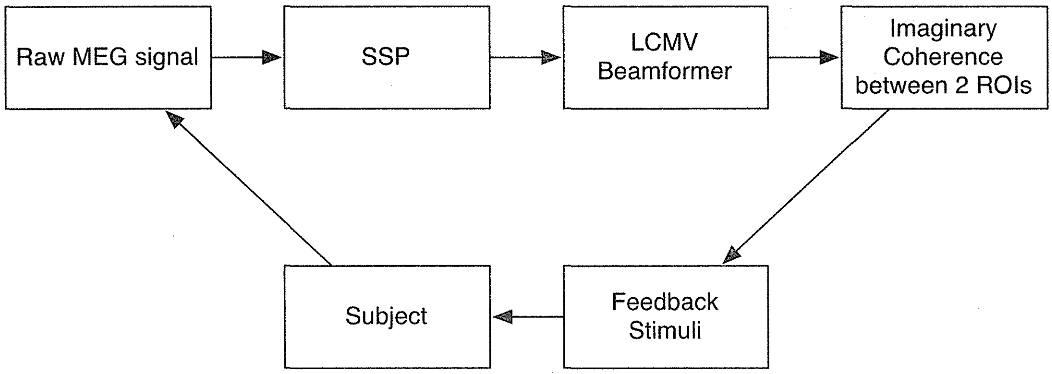

(a)

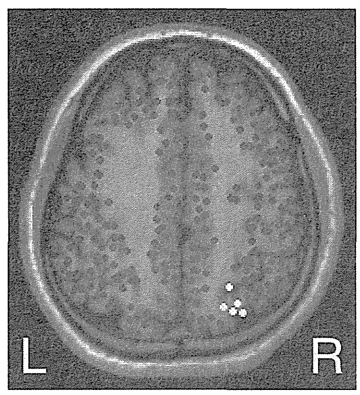

(b)

Fig. 2. (a) MEG signal processing. First, the raw MEG signals were processed using SSP for noise reduction. Then, the source time courses of each region of interest (ROI) were obtained using the LCMV beamformer and their imaginary coherence was computed to estimate the putative functional connectivity between the two ROIs. The feedback stimuli were then generated based on the calculated imaginary coherence. (b) Source locations were distributed across the gray matter (crosses). The yellow crosses indicate the source location for the right posterior parietal cortex (PPC) ROI. Each ROI location was determined as per Van Dijk *et al.* (2010).

coherence between them. The parameters (e.g., the radius of the circle) for the visual feedback stimuli were calculated based on the obtained imaginary coherence and then transmitted via a network link based on user diagram protocol (UDP) to the visual stimulation program (PsychoPy (Peirce, 2007) Version 1.73.04, University of Nottingham, UK). The program generated the visual stimuli based on the received parameters and transmitted them to the image projector. The data projector displayed the visual stimuli on a screen located in front of the subject, who was sitting in the MEG system.

2.2. *LCMV beamformer*

In this system, the MEG signal was reconstructed into an anatomical-location-based signal by applying the LCMV beamformer spatial filter (Van Veen & Kevin, 1988; Van Veen *et al.*, 1997). The combination of the LCMV beamformer spatial filter and the reconstruction of the cortical mantle from MRI anatomical image allowed the estimation of neural activity in the individual gray matter sheet. The LCMV beamformer spatial filter W was derived from the following formula:

$$W(q_0) = [H^T(q_0)C^{-1}(x)H(q_0)]^{-1}H^T(q_0)C^{-1}(x),$$

where q_0 is a location within the gray matter, C is the noise covariance matrix, x is MEG data for covariance matrix and H is the lead field matrix. An in-house MATLAB script was utilized to calculate W.

The lead field matrix was created using the following procedures. First, two T1-weighted images of the head of the subject were acquired and submitted to the FreeSurfer (Fischl *et al.*, 2001, 1999) cortical reconstruction process to obtain a surface model. A surface-based source space was created from the obtained surface model using MNE software (http://www.martinos.org/mne, Version 2.7.3 Build 3268 MacOSX-i386). For the volume conductor model, boundary element method (BEM)-meshes were created from the MRI T1 anatomical image. The position of the head in the MEG scanner was determined using four head position indicator (HPI) coils attached to the subject's head. The fiducial points were semi-automatically co-registered using "mne_analyze" (a tool in the MNE software) by manually identifying the left and right pre-auricular points and the nasion, and then optimizing the alignment of all digitized points with respect to the scalp surface. Finally, the lead-field matrix was calculated using MNE.

2.3. *Imaginary coherence*

The imaginary coherence was used to estimate the functional connectivity between two brain areas (Nolte *et al.*, 2004). Application of linear correlation or coherence metrics may result in false correlations reflecting spatial spread of a single source, the "true" correlation among brain regions usually contains a lag due to the finite speed of neural transmission. Thus, omitting the real part of the coherence is expected to remove false correlations. Imaginary coherence was defined as follows:

$$S_{ij}(f) \equiv \langle x_i(f)x_j^*(f)\rangle$$

where $S_{ij}(f)$ is a cross-spectrum of signals i and j. When $i = j$, S is the power spectrum and it is a real number. Coherency is defined as:

$$C_{ij}(f) \equiv \frac{S_{ij}(f)}{(S_{ii}(f)S_{jj}(f))^{\frac{1}{2}}}.$$

Coherence is the absolute value of coherency, that is,

$$\mathrm{Coh}_{ij}(f) \equiv |C_{ij}(f)|.$$

An in-phase spectral component is a real number, whereas, an out-of-phase spectral component is a complex number. Thus, retaining only the imaginary part of the cross-spectrum allows extraction of the lagged correlation component (Nolte *et al.*, 2004). This is called imaginary coherence. Namely,

$$\mathrm{ImCoh}_{ij}(f) \equiv |\mathrm{imag}(C_{ij}(f))|.$$

2.4. *MEG experiment*

We conducted a MEG experiment in one subject to validate our set-up. The subject was neurologically healthy and right-handed according to the Edinburgh inventory (Oldfield, 1971). The present study received approval from the Institutional Review Board of the National Rehabilitation Center for Persons with Disabilities, Tokorozawa, Japan. The subject provided written informed consent according to institutional guidelines. The subject sat comfortably in the MEG system in the upright position. A 2-min resting-state dataset was recorded for estimating the noise covariance matrix required for the construction of the LCMV beamformer spatial filter W. The sampling rate was 1000 Hz.

The visual stimuli were displayed in front of the subject (Fig. 3) and consisted of a circular green-and-blue checkerboard patch on the left, the fixation point inside the green feedback circle in the middle of the screen and a circular green-and-blue checkerboard patch on the right. The checkerboard patches flickered at 5 Hz or 6 Hz; when one checkerboard patch flickered at 5 Hz, the other flickered at 6 Hz. The number of trials at each frequency was counterbalanced. The subject was instructed to press a button (HHSC-2x4-C, fORP932, Current Designs Inc., Philadelphia, PA, USA) with his right index finger when focusing on the right checkerboard stimulus under the attend-right condition and to push the button with his left index finger when focusing on the left checkerboard stimulus under the attend-left condition. The subject was instructed to attend to the stimulus until an auditory cue was presented (at least 10 s), and he then rested for 10 s. During the experiment, the green circle in the center of the screen provided visual feedback; the radius changed according to the imaginary coherence between the right posterior parietal cortex ROI and left visual cortex ROI. Forty trials were performed under both the right- and left-attend conditions.

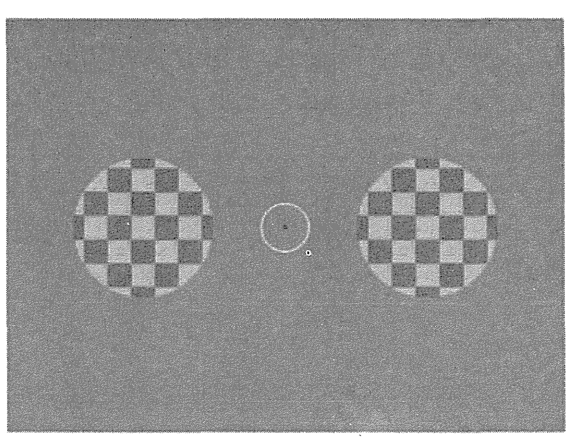

Fig. 3. Visual stimuli used in the MEG experiment. Green/blue checkerboard circles flickered at a specific frequency (5 Hz or 6 Hz). The green circle in the center provided the visual feedback and changed its radius according to the estimated functional connectivity between the right PPC and the left visual cortex.

Each ROI location was determined as by Van Dijk *et al.* (2010) (the posterior parietal cortex ROI was in the intraparietal sulcus) and was taken as a 3D sphere of 1 cm in radius. The value of each ROI at any time point was taken as the mean value of the vertices within the ROI. The imaginary coherence of the two time series with a temporal window size of 5 s was computed and integrated over frequencies 0–45 Hz, and the integrated value, multiplied by a constant, was used as the radius of the feedback circle.

The integrated imaginary coherence evaluated during the 10 s following the button press was used to index the difference in imaginary coherence between the two ROI pairs (right posterior parietal cortex (PPC) and left visual cortex, right (PPC) and right visual cortex). FFT window size was 2000 ms and the windows overlapped 1000 ms. Additionally, we used the right PPC and the left or right middle temporal cortex (V5/MT) as additional ROI pairs in the post-acquisition analysis.

3. Results

The present study investigated the putative functional connectivity between ROI pairs when the subject attended to the right flickering checkerboard stimulus. The ROI pairs consisted of the right PPC and the left or right visual cortex. Figure 4 shows the estimated functional connectivity based on the imaginary coherence of the

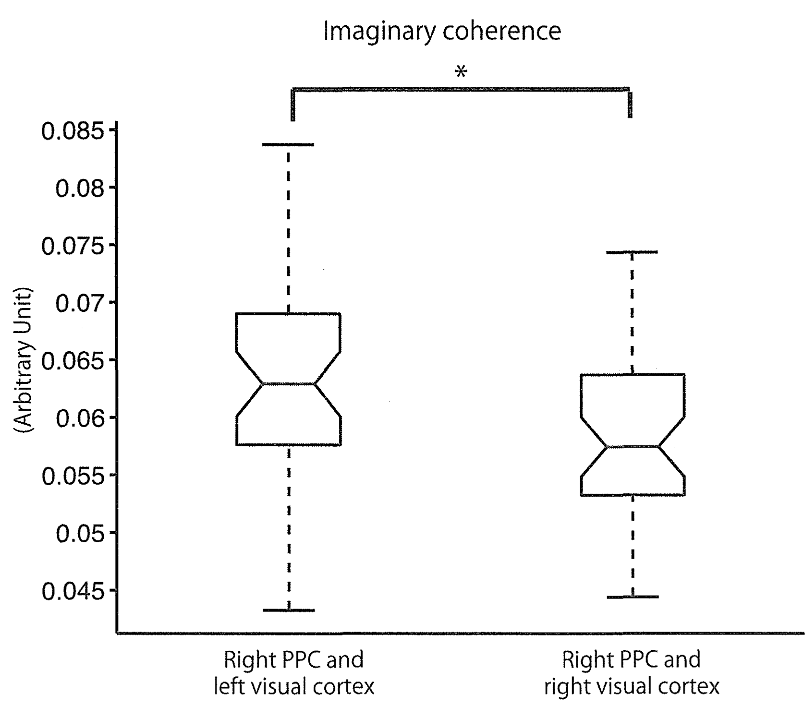

Fig. 4. Estimated functional connectivity according to the imaginary coherence of each ROI pair (the right PPC and the left and right visual cortex). The imaginary coherence (integrated over 0–45 Hz) between the right PPC and left visual cortex was greater than that between the right PPC and right visual cortex when the subject attended to the right checkerboard stimulus ($T_{39} = 2.5233$, $p = 0.0158$). The edges of each boxes are the 1st and 3rd quantiles, the whisker extends to $q3 + 1.5(q3 - q1)$ and $q1 - 1.5(q3 - q1)$ where, qn is the nth quantile.

two ROI pairs. The imaginary coherence between the right PPC and left visual cortex was greater than that between the right PPC and right visual cortex when the subject attended to the right checkerboard stimulus ($T_{39} = 2.5233$; $p = 0.0158$).

Additionally, we investigated the right PPC and the left or right middle temporal cortex (V5/MT) as ROI pairs. The imaginary coherence between the right PPC and left V5/MT was greater than that between the right PPC and right V5/MT ($T_{39} = 3.2129$; $p = 0.0026$; not shown in the figure.) Although the p-values were uncorrected, they remained significant after Bonferroni correction.

These findings indicate that functional connectivity between right PPC and left visual cortex changed when the subject attended to the right flickering checkerboard stimulus.

4. Discussion

We studied functional connectivity in the human brain by computing source-level coherence estimates in real-time from MEG data. We employed a beamformer to target specific brain regions (right PPC and visual cortices) and then evaluated functional connectivity between them by computing imaginary coherence between the corresponding source-level time series and provided visual feedback to the subject about the coherence estimate. Our rtMEG experiment showed that a healthy subject could increase coherence between the right PPC and the visual cortex while attending to a flickering visual stimulus.

4.1. *Methodological considerations*

We combined the beamformer technique and imaginary coherence for rtMEG neurofeedback. This combination allows estimation of the functional connectivity between two or more brain areas without the false correlations easily introduced by linear methods. In addition, this technique may reduce artifacts resulting from marked changes in head position within the sensor helmet over multiple neurofeedback training sessions as well as, improve generalization across multiple subjects and developmental changes in the brain during longitudinal studies in children.

4.2. *Neurophysiological background*

Increased putative functional connectivity, as measured by imaginary coherence, between the right PPC and the left visual cortex and between the right PPC and the left middle temporal area (MT/V5) was observed when the subject attended to the visual stimulus in the right hemifield. Our results are consistent with a previous fMRI experiment reporting functional connectivity between the primary visual cortex and MT/V5 and between the PPC and MT/V5 (Buchel & Friston, 1997). However, further investigation is necessary to explore the neurophysiological role of these brain areas in visual attention.

4.3. *Future applications*

rtMEG may have future applications in the context of brain–machine interface (BMI) or brain–computer interface (BCI) technologies. In BMI, one uses neurophysiological signals from the brain to control machines or computers. The technology has become wide spread in the past decade as a result of technical and mechanical improvements (Wolpaw *et al.*, 2002; Birbaumer & Cohen, 2007; Kansaku, 2011; Cichocki *et al.*, 2008). For rtMEG-based BMI, there are several potential applications such as training subjects to modulate specific spatial and dynamic features of their neural activity (Sudre *et al.*, 2011).

Moreover, rtMEG may be useful for neurofeedback training. Treatment using neurofeedback has been reported for psychiatric disorders such as ADHD (Fuchs *et al.*, 2003; Lofthouse *et al.*, 2012) and autism (Coben *et al.*, 2010). Functional and structural connectivity have been reported to be abnormal in the ADHD brain (Konrad & Eickhoff, 2010), and meta-analytic evidence suggests that neurofeedback treatment may be effective for children with ADHD (Arns *et al.*, 2009). Furthermore, neurofeedback training has been used in stroke rehabilitation (Soekadar *et al.*, 2011). The combination of beamformer techniques and imaginary coherence may provide the basis for effective neurofeedback training in which the patient is able to regulate the functional connectivity between two or more brain areas.

Acknowledgments

The present study was supported by a Ministry of Education, Culture, Sports, Science and Technology grant (#23300151) and a Ministry of Health, Labour and Welfare grant (#H22-011) to KK. We thank Drs. Y. Nakajima and F. Eto for their encouragement throughout the study.

REFERENCES

Arns, M., de Ridder, S., Strehl, U., Breteler, M. & Coenen, A. (2009) Efficacy of neurofeedback treatment in ADHD: The effects on inattention, impulsivity and hyperactivity: A meta-analysis. *Clin. EEG Neurosci.*, **40**, 180–189.

Birbaumer, N. & Cohen, L.G. (2007) Brain–computer interfaces: Communication and restoration of movement in paralysis, *J. Physiol. (Lond.)*, **579**, 621–636.

Birbaumer, N., Elbert, T., Canavan, A.G. & Rockstroh, B. (1990) Slow potentials of the cerebral cortex and behavior. *Physiol. Rev.*, **70**, 1–41.

Buch, E., Weber, C., Cohen, L.G., Braun, C., Dimyan, M.A., Ard, T., Mellinger, J., Caria, A., Soekadar, S., Fourkas, A. & Birbaumer, N. (2008) Think to move: A neuromagnetic brain–computer interface (BCI) system for chronic stroke. *Stroke*, **39**, 910–917.

Buchel, C. & Friston, K.J. (1997) Modulation of connectivity in visual pathways by attention: Cortical interactions evaluated with structural equation modelling and fMRI. *Cereb. Cortex*, **7**, 768–778.

Caria, A., Sitaram, R., Birbaumer, N. (2012) Real-time fMRI: A tool for local brain regulation. *Neuroscientist*, **18**, 487–501.

Cichocki, A., Washizawa, Y., Rutkowski, T., Bakardjian, H., Phan, A.H., Choi, S., Lee, H., Zhao, Q.B., Zhang, L.Q. & Li, Y.Q. (2008) Noninvasive BCIs: Multiway signal-processing array decompositions. *Computer*, **41**, 34–42.

Coben, R., Linden, M. & Myers, T.E. (2010) Neurofeedback for autistic spectrum disorder: A review of the literature. *Appl. Psychophysiol. Biofeedback*, **35**, 83–105.

Fischl, B., Liu, A. & Dale, A.M. (2001) Automated manifold surgery: Constructing geometrically accurate and topologically correct models of the human cerebral cortex. *IEEE Trans. Med. Imaging*, **20**, 70–80.

Fischl, B., Sereno, M.I. & Dale, A.M. (1999) Cortical surface-based analysis. Ii: Inflation, flattening, and a surface-based coordinate system. *Neuroimage*, **9**, 195–207.

Fuchs, T., Birbaumer, N., Lutzenberger, W., Gruzelier, J.H. & Kaiser, J. (2003) Neurofeedback treatment for attention-deficit/hyperactivity disorder in children: A comparison with methylphenidate. *Appl. Psychophysiol. Biofeedback*, **28**, 1–12.

Kamiya, J. (1968) Conscious control of brain waves. *Psychol. Today*, **1**, 57–60.

Kansaku, K. (2011) Brain–machine interfaces for persons with disabilities. In: K. Kansaku and L.G. Cohen, eds. *Systems Neuroscience and Rehabilitation*. Japan: Springer, pp. 19–33.

Konrad, K. & Eickhoff, S.B. (2010) Is the ADHD brain wired differently? A review on structural and functional connectivity in attention deficit hyperactivity disorder. *Hum. Brain Mapp.*, **31**, 904–916.

Lofthouse, N., Arnold, L.E., Hersch, S., Hurt, E. & DeBeus, R. (2012) A review of neurofeedback treatment for pediatric ADHD. *J. Attention Disord.*, **16**, 351–372.

Mellinger, J., Schalk, G., Braun, C., Preissl, H., Rosenstiel, W., Birbaumer, N. & Kubler, A. (2007) An MEG-based brain–computer interface (BCI). *Neuroimage*, **36**, 581–593.

Nolte, G., Bai, O., Wheaton, L., Mari, Z., Vorbach, S. & Hallett, M. (2004) Identifying true brain interaction from EEG data using the imaginary part of coherency. *Clin. Neurophysiol.*, **115**, 2292–2307.

Oldfield, R.C. (1971) The assessment and analysis of handedness: The Edinburgh inventory. *Neuropsychologia*, **9**, 97–113.

Oostenveld, R., Fries, P., Maris, E. & Schoffelen, J.M. (2011) Fieldtrip: Open source software for advanced analysis of MEG, EEG, and invasive electrophysiological data. *Comput. Intell. Neurosci.*, **2011**, 156869.

Peirce, J.W. (2007) Psychopy — psychophysics software in python. *J. Neurosci. Methods*, **162**, 8–13.

Sacchet, M.D., Mellinger, J., Sitaram, R., Braun, C., Birbaumer, N. & Fetz, E. (2012) Volitional control of neuromagnetic coherence. *Front. Neurosci.*, **6**, 189.

Shibata, K., Watanabe, T., Sasaki, Y. & Kawato, M. (2011) Perceptual learning incepted by decoded fMRI neurofeedback without stimulus presentation. *Science*, **334**, 1413–1415.

Siegel, M., Donner, T.H. & Engel, A.K. (2012) Spectral fingerprints of large-scale neuronal interactions. *Nat. Rev. Neurosci.*, **13**, 121–134.

Soekadar, S.R., Birbaumer, N. & Cohen, L.G. (2011) Brain–computer interfaces in the rehabilitation of stroke and neurotrauma. In: K. Kansaku and L.G. Cohen, eds. *Systems Neuroscience and Rehabilitation*. Japan: Springer, pp. 3–18.

Sudre, G., Parkkonen, L., Bock, E., Baillet, S., Wang, W. & Weber, D.J. (2011) rtMEG: A real–time software interface for magnetoencephalography. *Comput. Intell. Neurosci.*, **2011**, 327953.

Van Dijk, K.R., Hedden, T., Venkataraman, A., Evans, K.C., Lazar, S.W. & Buckner, R.L. (2010) Intrinsic functional connectivity as a tool for human connectomics: Theory, properties, and optimization, *J. Neurophysiol.*, **103**, 297–321.

Van Veen, B.D. & Kevin, M.B. (1988) Beamforming: A versatile approach to spatial filtering. *IEEE ASSP Magazine*, 4–24.

Van Veen B.D., Van Drongelen, W., Yuchtman, M. & Suzuki, A. (1997) Localization of brain electrical activity via linearly constrained minimum variance spatial filtering. *IEEE Trans. Biomed. Eng.*, **44**, 867–880.

Weiskopf, N., Veit, R., Erb, M., Mathiak, K., Grodd, W., Goebel, R. & Birbaumer, N. (2003) Physiological self-regulation of regional brain activity using real–time functional magnetic resonance imaging (fMRI): Methodology and exemplary data. *Neuroimage*, **19**, 577–586.

Wolpaw, J.R., Birbaumer, N., McFarland, D.J., Pfurtscheller, G. & Vaughan, T.M. (2002) Brain-computer interfaces for communication and control. *Clin. Neurophysiol.*, **113**, 767–791.

平成 25 年度厚生労働科学研究費補助金（障害者対策総合研究事業（身体・知的等分野））
「ブレインーマシン・インターフェイス（BMI）による障害者自立支援機器の開発」

総括・分担研究報告書

発行者　　中島　八十一（研究代表者：国立障害者リハビリテーションセンター）
〒359-8555　埼玉県所沢市並木 4-1